



# Stokes Flow in a Z-Shaped Cavity With Moving Upper Lid

*Üst Kapağı Hareketli Z-Şekilli Kavitedeki Stokes Akış*

Ebutalib Çelik<sup>1\*</sup> , Murat Luzum<sup>2</sup> , Ali Deliceoğlu<sup>3</sup> 

<sup>1</sup>Çanakkale Onsekiz Mart University, Vocational School of Technical Sciences, Department of Computer Technologies, Canakkale, Turkey

<sup>2</sup>Van Yüzüncü Yıl University, Science Faculty, Department of Mathematics, Van, Turkey

<sup>3</sup>Erciyes University, Science Faculty, Department of Mathematics, Kayseri, Turkey

## Abstract

Flow patterns and their bifurcation for a steady, viscous, Stokes flow inside a Z-shaped cavity with moving upper lid are investigated. Stokes equation with two parameters  $h_1$  and  $h_2$  which are related to the heights of the field is solved analytically using an infinite series of eigenfunctions. The  $(h_1, h_2)$  control space diagram is constructed to examine the new eddy generation, and attention is then focused on the effect of the re-entrant corner on the flow transformation in the Z-shaped domain.

**Keywords:** Eddy generation, Flow bifurcation, Single-lid, Z-shaped cavity

## Öz

Durağan, viskoz, Stokes akış için üst kapağı hareketli Z şekilli bir kaviti içindeki akış modelleri ve çatallanmaları araştırılmıştır. Bölge yükseklikleri ile ilgili iki parametre  $h_1$  ve  $h_2$  olmak üzere Stokes denklemi, öz fonksiyonların sonsuz serisi kullanılarak analitik olarak çözülmüştür.  $(h_1, h_2)$  kontrol uzay diyagramı yeni girdap oluşumunu incelemek için oluşturulmuştur ve daha sonra, çıkıntılı köşenin Z-şekilli alandaki akış dönüşümü üzerindeki etkisine odaklanılmıştır.

**Anahtar Kelimeler:** Girdap oluşumu, Akış çatallanmaları, Tek kapaklı, Z-şekilli kaviti

## 1. Introduction

Cavity type problems are such evergreen research topic which has been studied for many years in different fields of mathematics and engineering including aerodynamic applications (Olsmann and Colonius 2011, Yang et al. 2014), coating flow (Gaskell et al. 1995, Hellebrand 2006), heat transfer (Mahmoodi 2011, Oztop and Dagtekin 2004), biological process (Sheu and Chiang 2014). Lid-driven cavity flow problems are the most common of these topics. Studies on the cavity flow can be categorized into two main issues: computational fluid dynamics (CFD) and qualitative properties of streamlines.

In computational view, there are many studies in the literature on testing new algorithms and numerical methods developed for non-zero Reynolds flow (An et al. 2019,

Botella and Peyret 1998, Bruneau and Saad 2006, Erturk et al. 2005). Recently, (Erturk 2018) solved the 2-D steady incompressible annular cavity flow using an efficient numerical method which can obtain solutions at high Reynolds numbers and compared the results with those in the previous study. (Hriberšek and Škerget 2005) presented new advances in the boundary domain integral method (BDIM) for computation of viscous fluid flows, governed by the Navier–Stokes equations. They tested the accuracy of the new numerical algorithm for several problems, including the standard driven cavity with up to  $Re = 10000$ , driven an L shaped cavity with up to  $Re = 7500$  and flow in a Z shaped channel with up to  $Re = 400$ .

Studies examining the qualitative properties of the streamline are related to vortex formation, flow bifurcation and local analysis of streamline. For example, (Bakker 1991) used a Taylor series expansion of the velocity vector field to investigate flow topology and structural stability of flow patterns near a critical point on a stationary wall. (Brøns and Hartnack 1999) revealed flow structure near a

\*Corresponding author: [ecelik@erciyes.edu.tr](mailto:ecelik@erciyes.edu.tr)

Ebutalib Çelik  [orcid.org/0000-0002-4500-4465](https://orcid.org/0000-0002-4500-4465)

Murat Luzum  [orcid.org/0000-0001-6256-0597](https://orcid.org/0000-0001-6256-0597)

Ali Deliceoğlu  [orcid.org/0000-0003-0863-6276](https://orcid.org/0000-0003-0863-6276)

simple degenerate critical points away from boundaries by using normal form transformations which are a tool for eliminating the higher-order terms in the stream functions. (Hartnack 1999) also used the same method for critical points which is closed to a fixed wall. Recently, (Deliceoğlu et al. 2019) made a local analysis of the vector field by simplified the streamlines of the Hamiltonian system using the homotopy invariance of the index theory. Then, as a theoretical framework, they considered an L-shaped cavity with lids moving in the same directions to determine the sequence of flow structures by which eddies are generated.

As a closed flow domain, a rectangular cavity is the most probably preferred due to the simplicity of the application of the boundary conditions. Some of the significant studies included the rectangular cavity is (Gürcan 2003, Gürcan et al. 2003, Gürcan et al. 2006, Shankar 1993). In addition to the rectangular, flow structures and bifurcations in different types of shapes, such as annular, L-shaped, T-shaped, have been of interest. (Gaskell et al. 1997) formulated a boundary value problem which is solved for the stream function  $\psi$  for a half-filled annulus. They showed that the flow domain consists of two (one) large eddies (eddy), each having a stagnation point on the centerline for both counter-rotating  $S < 0$  and co-rotating  $S > 0$  cases. As  $A$  and  $S$  are varied, there is a change in the flow structure of the stationary point such that it turns into a saddle from a center or vice versa. (Gürcan et al. 2016) analyzed the Stokes flow within the annular region formed by a pair of stationary side walls surrounded by straight lids moving in the opposite direction. They identified that after various flow transformations in the area, the new eddy appeared and was fully developed for  $S \in [-1, 0)$  and  $A \in [1.6, 6.5)$ .

(Deliceoğlu and Aydin 2013) investigated flow transformation and eddy genesis in a steady, viscous L-shaped cavity with the lids moving in opposite directions by Galerkin finite element method with a stabilization technique. They focused on the flow transformation as well as the effect of the corner point on the vortex formation and observed an unprecedented separation bubble around the re-entrant corner point. Also, by taking  $Re = 500$ , they found that the Reynolds number accelerated the formation of new vortices in the upper part of the cavity. In the following, (Deliceoğlu and Aydin 2014) presented flow patterns formed by varying cavity heights in the L-shaped region with a moving single lid. For  $-1.4 < h_1 < 0$  and  $0.1 < h_2 < 3.2$ , they obtained the  $(h_1, h_2)$  parameter space which is formed by the bifurcation curves expressing the

transformation of structure at the critical point. Recently, (Deliceoğlu and Çelik 2019) studied the viscous flow in the T-shaped domain where the upper lid governs the flow. They construct the  $(h_1, h_2)$  control space diagram to show new vortex formation scenarios.

In this study, unlike the above geometries, the flow topology in the Z-shaped region with a single lid is examined. To do this, boundary value problem is formed and Stokes equation governing the flow is solved analytically. Flow patterns in the region are obtained by changing the parameters of lower cavity height  $h_1$  and upper cavity height  $h_2$ , and the effect of separating lines near the corner points on the formation of new vortex is investigated.

## 2. Material and Methods

A two-dimensional Z-shaped cavity with boundary condition is shown in Figure 1. The cavity is filled with an incompressible fluid, and it is assumed that the width of the cavity is fixed and all walls, except the upper lid with horizontal motion, are stationary. The flow is driven by the motion of the upper lid with constant speed  $u = 1$ . Under the Stokes approximation, the equations of motion reduce to the biharmonic equation for the stream function

$$\frac{\partial^4 \psi}{\partial x^4} + 2 \frac{\partial^4 \psi}{\partial x^2 \partial y^2} + \frac{\partial^4 \psi}{\partial y^4} = \nabla^4 \psi(x, y) = 0 \quad (1)$$

The velocity components are obtained by derivatives of stream function  $\psi$

$$u = \frac{\partial \psi}{\partial y} \quad v = -\frac{\partial \psi}{\partial x} \quad (2)$$

The no-slip boundary conditions for the upper lid and seven fixed walls can be written by using the relations (2) in terms of derivatives of the stream function as follow:

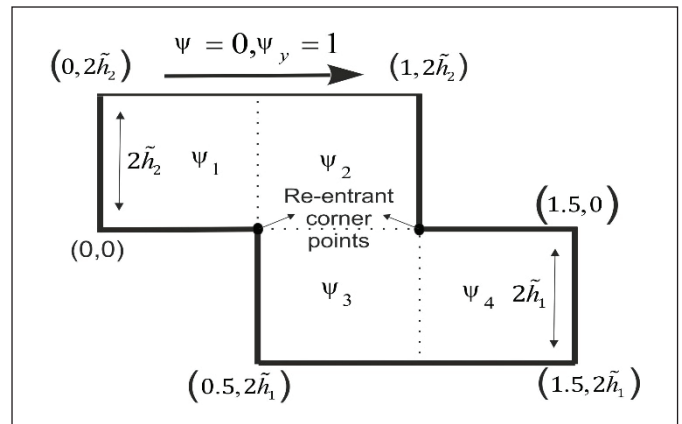


**Figure 1.** Boundary conditions for a lid-driven Z-shaped cavity.

$$\begin{aligned}
 & \frac{\partial \psi}{\partial y}(x, 2\tilde{h}_2) = 1, (0 \leq x \leq 1), \frac{\partial \psi}{\partial x}(0, y) \\
 & = 0, (0 \leq y \leq 2\tilde{h}_2), \frac{\partial \psi}{\partial y}(x, 0) = 0, (0 \leq x \leq 0.5) \\
 & \frac{\partial \psi}{\partial y}(x, 2\tilde{h}_1) = 0, (0.5 \leq x \leq 1.5), \frac{\partial \psi}{\partial x}(1.5, y) \\
 & = 0, (2\tilde{h}_1 \leq y \leq 0), \frac{\partial \psi}{\partial y}(x, 0) = 0, (1 \leq x \leq 1.5) \\
 & \frac{\partial \psi}{\partial x}(0.5, y) = 0, (2\tilde{h}_1 \leq y \leq 0), \frac{\partial \psi}{\partial x}(1, y) = 0, (0 \leq y \leq 2\tilde{h}_2),
 \end{aligned} \tag{3}$$

The boundary value problem formed for the cavity can be solved analytically or numerically. In this paper, we solve the biharmonic equation using Papkovitch-Fadle eigenfunctions, which arise from the separation of variables. The region is divided into simple sub-regions and the stream function is defined for each sub-region in terms of these eigenfunctions which satisfy all the sidewall conditions. By applying these boundary conditions to the eigenfunctions, a linear equation system consisting of unknown coefficients is obtained.

The stream function for the first region can be written as:

$$\begin{aligned}
 & \psi_1(x, y) \\
 & = \sum_{n=-\infty}^{\infty} \frac{\phi_{a,n}(x)}{\lambda_{a,n}^2} \left( \frac{a_n \sinh(\lambda_{a,n}(y - \tilde{h}_2))}{\sinh(\lambda_{a,n}\tilde{h}_2)} + \frac{b_n \cosh(\lambda_{a,n}(y - \tilde{h}_2))}{\cosh(\lambda_{a,n}\tilde{h}_2)} \right) \\
 & + \frac{\phi_{s,n}(x)}{\lambda_{s,n}^2} \left( \frac{c_n \sinh(\lambda_{s,n}(y - \tilde{h}_2))}{\sinh(\lambda_{s,n}\tilde{h}_2)} + \frac{d_n \cosh(\lambda_{s,n}(y - \tilde{h}_2))}{\cosh(\lambda_{s,n}\tilde{h}_2)} \right) \\
 & + \frac{\xi_{a,n}(y)}{\mu_{a,n}^2} \left( \frac{e_n \sinh(\mu_{a,n}(x - 0.25))}{\sinh(0.25\mu_{a,n})} + \frac{f_n \cosh(\mu_{a,n}(x - 0.25))}{\cosh(0.25\mu_{a,n})} \right) \\
 & + \frac{\xi_{s,n}(y)}{\mu_{s,n}^2} \left( \frac{g_n \sinh(\mu_{s,n}(x - 0.25))}{\sinh(0.25\mu_{s,n})} + \frac{h_n \cosh(\mu_{s,n}(x - 0.25))}{\cosh(0.25\mu_{s,n})} \right).
 \end{aligned} \tag{4}$$

where the functions,

$$\begin{aligned}
 & \phi_{a,n}(x) = s_{a,n}(\sin(s_{a,n})\cos(s_{a,n}(4x - 1)) \\
 & - (4x - 1)\cos(s_{a,n})\sin(s_{a,n}(4x - 1))),
 \end{aligned} \tag{5}$$

$$\begin{aligned}
 & \phi_{s,n}(x) = s_{s,n}(\cos(s_{s,n})\sin(s_{s,n}(4x - 1)) \\
 & - (4x - 1)\sin(s_{s,n})\cos(s_{s,n}(4x - 1))),
 \end{aligned} \tag{6}$$

$$\begin{aligned}
 & \xi_{a,n}(y) \\
 & = s_{a,n} \left[ \begin{aligned} & \sin(s_{a,n})\cos\left(\frac{s_{a,n}(y - \tilde{h}_2)}{\tilde{h}_2}\right) \\ & - \frac{(y - \tilde{h}_2)\cos(s_{a,n})}{\tilde{h}_2}\sin\left(\frac{s_{a,n}(y - \tilde{h}_2)}{\tilde{h}_2}\right) \end{aligned} \right],
 \end{aligned} \tag{7}$$

$$\begin{aligned}
 & \xi_{s,n}(y) \\
 & = s_{s,n} \left[ \begin{aligned} & \cos(s_{s,n})\sin\left(\frac{s_{s,n}(y - \tilde{h}_2)}{\tilde{h}_2}\right) \\ & - \frac{(y - \tilde{h}_2)\sin(s_{s,n})}{\tilde{h}_2}\cos\left(\frac{s_{s,n}(y - \tilde{h}_2)}{\tilde{h}_2}\right) \end{aligned} \right],
 \end{aligned} \tag{8}$$

are the symmetric and anti-symmetric eigenfunctions, respectively (Fadle 1940, Papkovich 1970). The sidewall boundary conditions (3) are used to obtain the eigenvalues  $s_{a,n}$  and  $s_{s,n}$  which satisfy the following equations:

$$\sin(2\lambda_{a,n}) = -2\lambda_{a,n}, \sin(2\lambda_{s,n}) = -2\lambda_{s,n}. \tag{9}$$

The eigenvalues are determined by the Newton iteration procedure described by (Robbins and Smith 1948). Similarly, the stream function can be derived for the other sub-regions. Finally, stream function  $\psi(x, y)$  for the domain is given by

$$\psi(x, y) = \psi_1(x, y) + \psi_2(x, y) + \psi_3(x, y) + \psi_4(x, y). \tag{10}$$

This solution procedure was used by (Driesen et al. 1998, Trogdon and Joseph 1982).

### 3. Results

In this section, the vortex formation mechanism in the Z-shaped cavity with upper-lid moving horizontal directions will be examined. In the next part of the article, for the sake of convenience it is assume that  $2\tilde{h}_1 = h_1$  and  $2\tilde{h}_2 = h_2$ . A lower part of cavity height  $h_1$  and upper part of cavity height  $h_2$  are considered as a parameter. The topological structure of the degenerate critical point within the region changes as the heights of the parameters vary. This transformation occurs from the saddle to the centre or vice versa for incompressible flow and is expressed in terms of flow bifurcation in fluid dynamics.

Using the analytical solution of the Stokes equation in Section 2, a  $(h_1, h_2)$  parameter space (bifurcation diagram), which includes the curves representing flow bifurcations is generated (Figure 2).  $h_1$  is fixed, while  $h_2$  is changing or vice versa to obtain all bifurcation curves. It is sufficient to consider parameters in the range of  $-2.8 < h_1 < 0.1, 0 < h_2 < 2$ , to examine flow transformations which increase the number of vortices in the region. In this range, the parameter space contains a set of the co-dimension-bifurcation curve, and each curve represents the flow bifurcation at degenerate critical points.

#### 3.1. Streamline Topologies Near a Stationary Wall

In the literature, degenerate critical points are classified as simple or non-simple depending on the Jacobian matrix of the velocity field. (Hartnack 1999) studied local flow topology at a simple degenerate critical point which has a singular and non-zero Jacobian matrix. Moreover, he used the generation function to simplify the fourth-order terms of the stream function in the normal form approach. We skip computational ways and only give the following theorem

for the stream function of codimension one. A detailed description of the method is found in (Hartnack 1999).

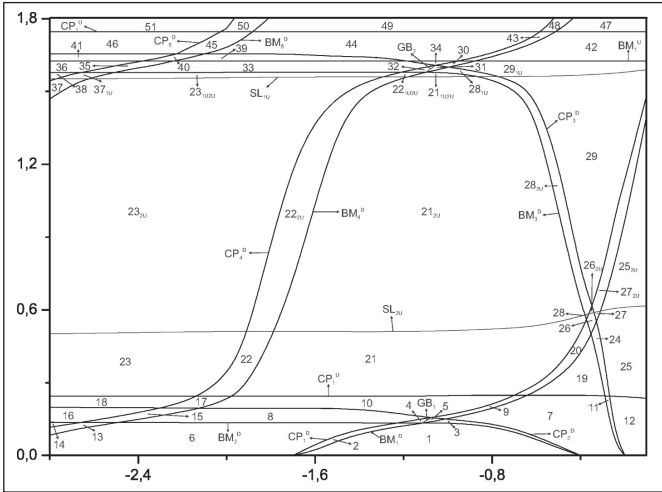


**Figure 2.** The control space diagram is divided into different regions by bifurcation curves. Flow patterns in Figure 5-7 are correspond to these regions.

**Theorem 1:** Let  $\psi$  is expanded in a power series

$$\psi = y^2 \sum_{i+j=0}^{\infty} a_{i,j+2} x^i y^j \quad (11)$$

Assuming the non-degenerate conditions  $a_{0,3} \neq 0, a_{2,2} \neq 0$  a normal form of order 4 for the stream function is

$$\psi = y^2 \left( \sigma y + \mu + \frac{1}{2} x^2 \right) \quad (12)$$

where

$$\sigma = \begin{cases} 1 & \text{for } \frac{a_{2,2}}{a_{0,3}} > 0 \\ -1 & \text{for } \frac{a_{2,2}}{a_{0,3}} < 0 \end{cases} \quad (13)$$

and  $\mu$  is a transformed small parameters.

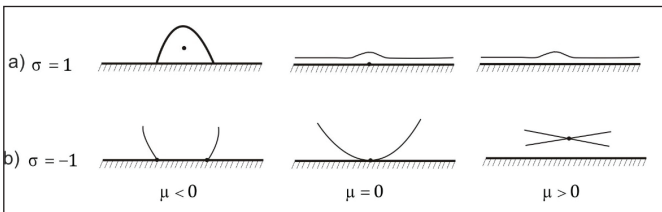


**Figure 3.** Local streamlines near the wall for a)  $\sigma = 1$  b)  $\sigma = -1$ .

**Theorem 2:** Let  $a_{1,0}, a_{0,1}, a_{2,0}, a_{1,1}$  and  $\tilde{a}_{3,0}, \dots, \tilde{a}_{N-1,0}$  be small parameters. Assuming the non-degeneracy conditions  $a_{0,2} \neq 0, \tilde{a}_{N,0} \neq 0$  normal formal of order N for the stream function is

$$\psi_N = \frac{\sigma}{2} y^2 + f(x) \quad f(x) = \sum_{i=1}^N c_i x^i \quad c_{N-1} = 0, c_N = \frac{1}{N} \quad (14)$$

where

$$\sigma = \begin{cases} -1 & \text{for } N \text{ even and } a_{0,2}/\tilde{a}_{N,0} < 0 \\ 1 & \text{for } N \text{ even and } a_{0,2}/\tilde{a}_{N,0} > 0 \text{ or } N \text{ odd} \end{cases} \quad (15)$$

and  $c_i, i = 1, \dots, N - 2$  are transformed small parameters.

### 3.2 Forming Control Space Diagram and Eddy Generation

The curves in the control space diagram are named according to the bifurcation type. The lower index shows the number of bifurcation, while the upper index indicates the place which part of the cavity bifurcation occurs (Up or Down). Three types of flow bifurcation, one on the wall and the others inside the flow, are observed during the study flow bifurcation. The first type, the two saddle points on the wall approach and, then coalesce with each other at one point on the wall to produce a saddle in the flow (Figure 3-(b)). This bifurcation is shown in the diagram by BM (bubble merging). The second type of bifurcation occurs inside the flow where the degenerate critical point is bifurcated to a saddle with a centre point (Figure 4). This type of bifurcation is called CP (cusp-bifurcation). Sometimes the topological structure of the flow transformation to another form, but there is no change in the number of critical points, such transformations are labelled with GB (global). All curves divide the bifurcation diagram ( $h_1, h_2$ ) into 51 different regions as shown in Figure 2, and all flow patterns in each region are shown in the Figure 5-7.

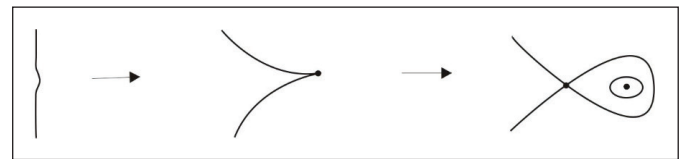


**Figure 4.** Bifurcation series of the degenerate point inside the flow for  $N = 3$  in Eq. (14).

This study aims to show how critical points turn into vortex after a series of structural bifurcations. For example, the lower region numbered with (1) contains one large vortex with inner separatrix. By changing the parameters,  $h_1$  and  $h_2$ , the lower corner vortices combine to form a new separatrix structure along the BM curve (zone 2). When  $h_2$  is fixed and moved to zone 6, this structure leaves its place in the vortex after  $CP_1$  bifurcation. This basic transformation series is exactly equivalent to the series obtained by (Gürçan 2005) for the rectangular cavity with the upper

lid. However, unlike the rectangular cavity, surprisingly, the same bifurcation series also occurs on the right wall of the lower region ( $1 \rightarrow 3 \rightarrow 7$ ). After the same sequence of

bifurcations, the vortices on the bottom wall or the right wall generates a full vortex with the corners at the lower part of cavity. These bifurcation are shown in Figure 8.

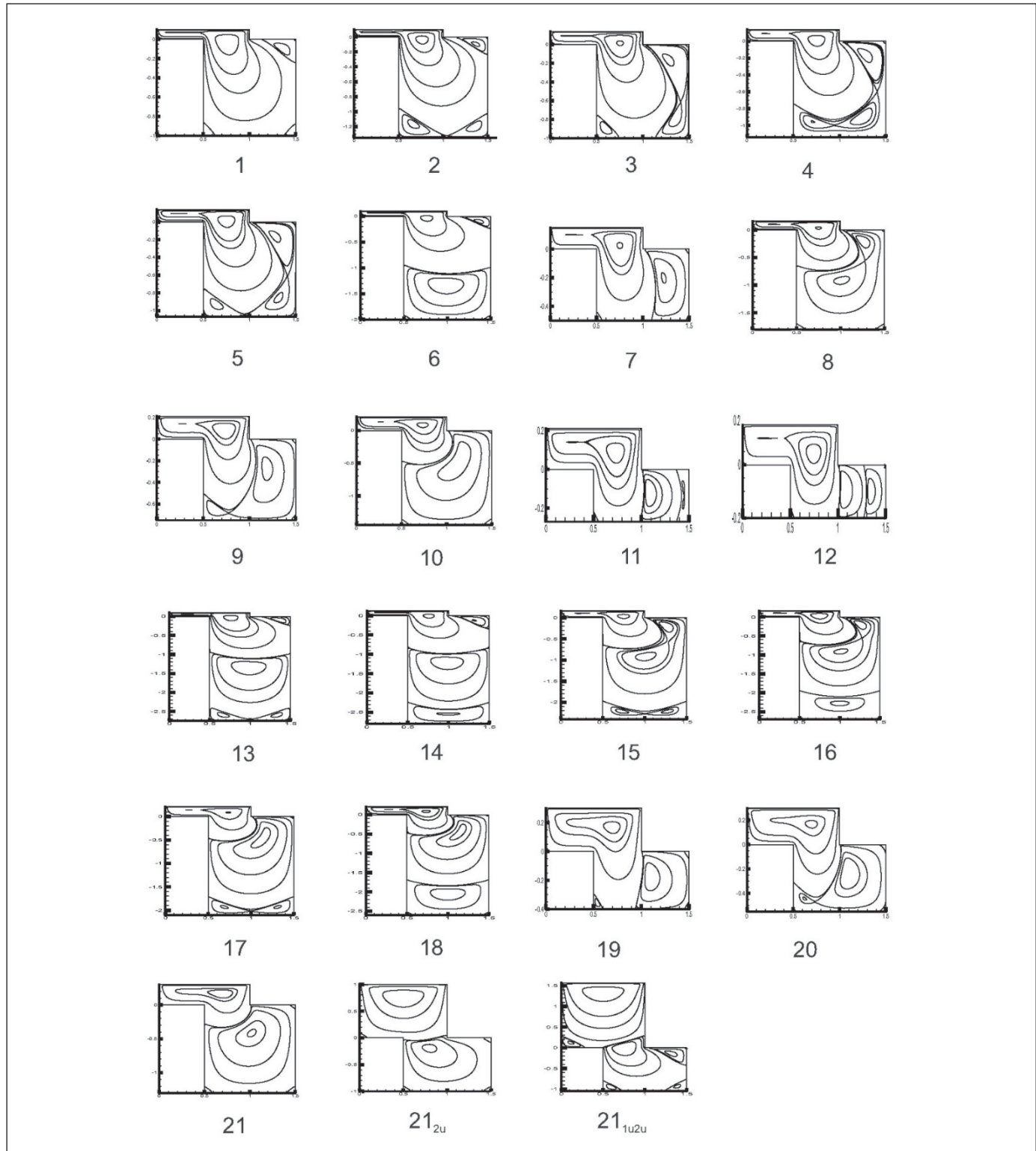


Figure 5. Schematic representation of the streamlines formed in each region in the control space diagram.

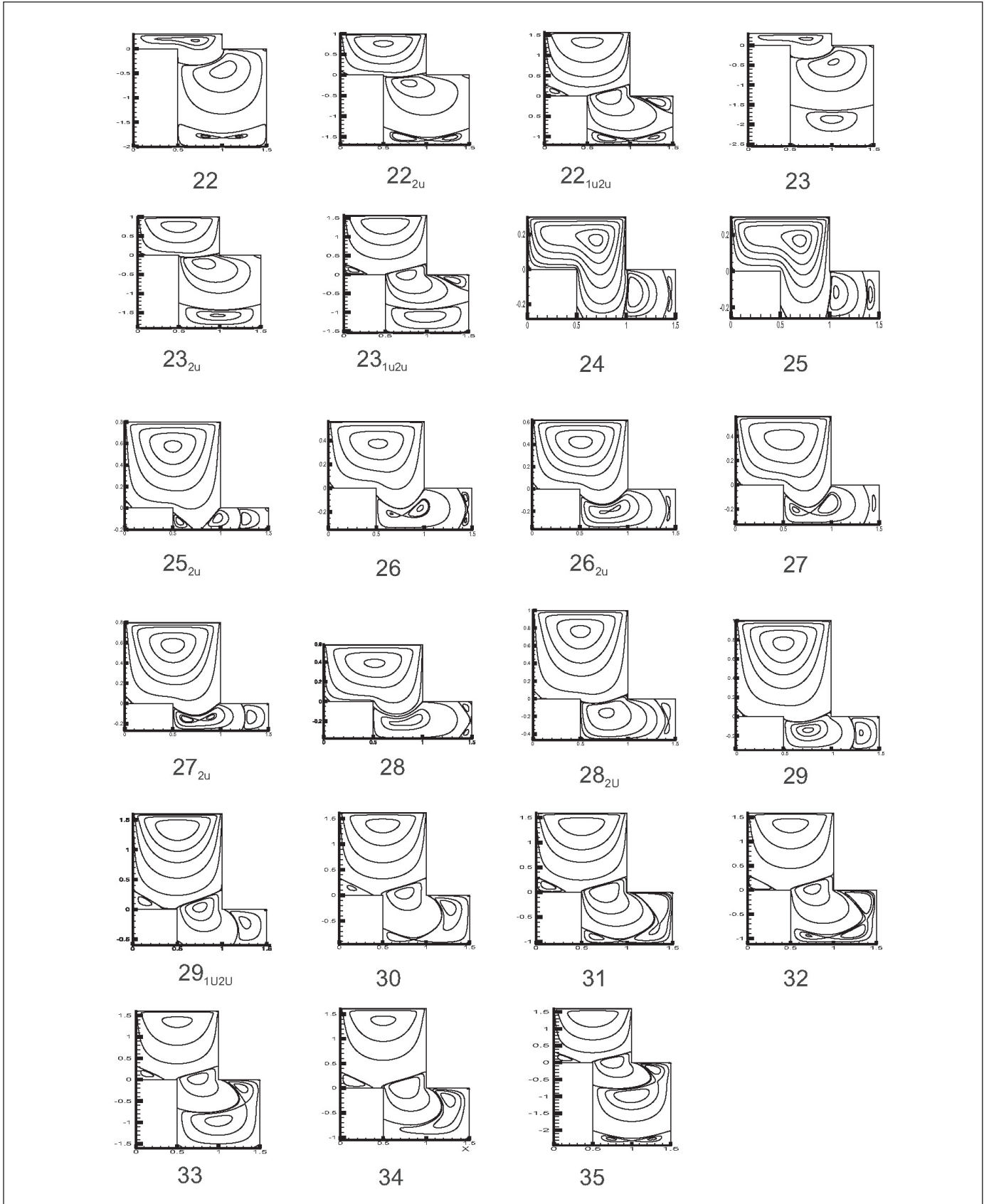


Figure 6. Schematic representation of the streamlines formed in each region in the control space diagram (continued).

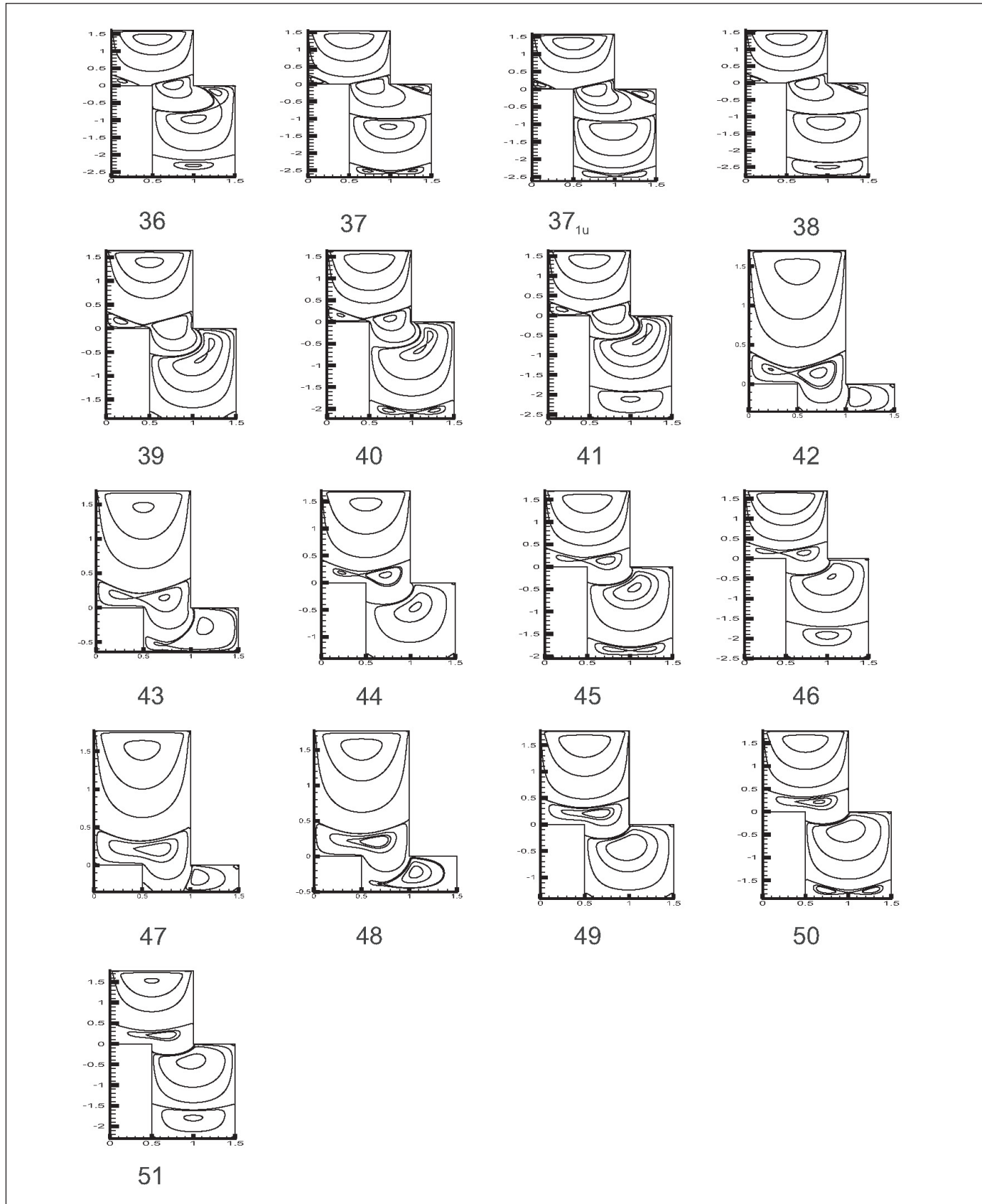
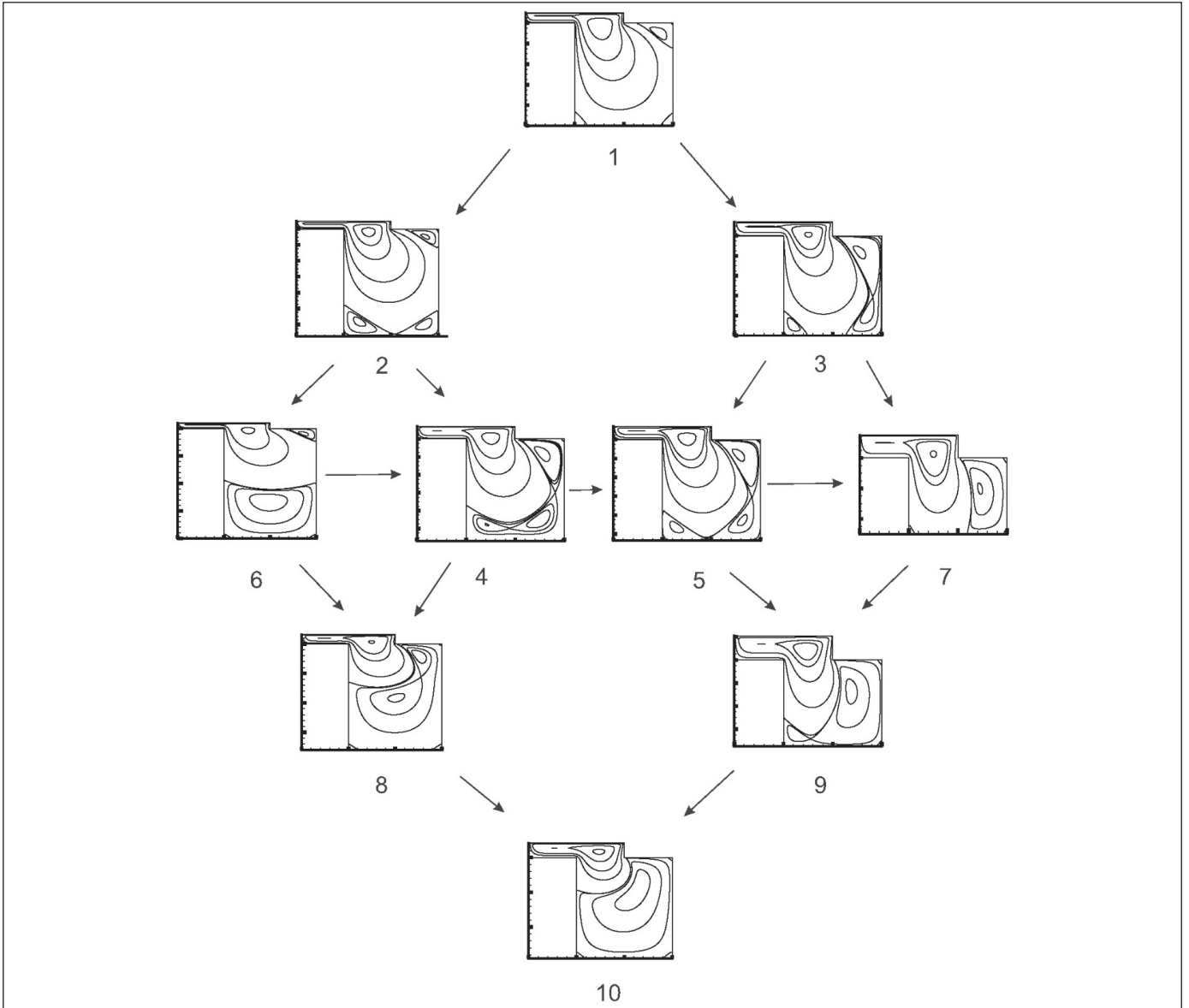


Figure 7. Schematic representation of the streamlines formed in each region in the control space diagram (continued).



**Figure 8.** Eddy generation at the lower part of the cavity by increasing  $h_1$ .

Let us continue to examine the control space diagram by studying the role of the right corner point in the vortex formation. First, there are two primary vortices in the domain, and the separation line is on the horizontal wall (Figure 9-(19)). Flow transformation (19 → 24 → 25) shows that the lower-right part of the cavity acts as a rectangular cavity. Just before the separation line crosses the corner point, it joins with the left-lower corner vortex of the cavity to form a separatrix. After the separation line crosses the corner point, the value of  $h_2 \approx -0.55$ , the separatrix in the region leaves its place in a full vortex, and the vortex formation is completed at the bottom of the cavity (Figure 9).

So far, the separation line is below the left corner, and new vortices are formed in the lower-middle part of the cavity. When the  $h_2$  is fixed and moved horizontally between zones (29-37) in the diagram, structural bifurcation occurs at the bottom of the cavity. In the control space, when  $h_1$  is fixed, and  $h_2$  is increased, the bifurcation curve  $SL_{1,1'}$  which refers to the separation line passing the corner point, is first seen. This indicates that the separation line crosses the corner point before the changes in topological structure over the upper part of the cavity. Indeed, when the parameter space is examined, the separation line crosses the corner point firstly and then joins with the corner vortex on the upper cavity.

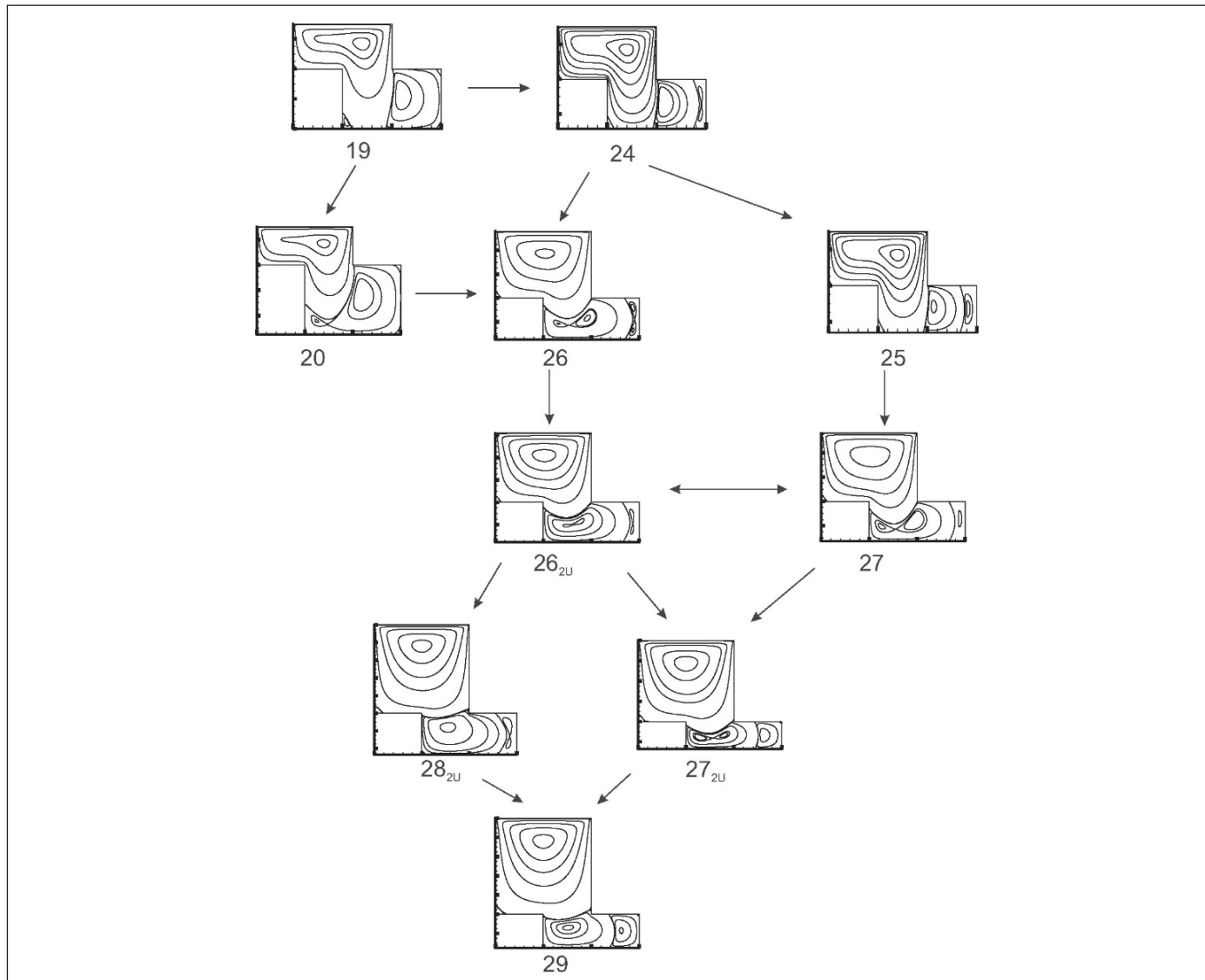


**Figure 9.** The role of the separation line on the effect of eddy formation.

This value is constant regardless of  $h_1$  and is approximately  $h_2=1.626$ . When the length of the upper part of the cavity is further increased, the number of vortices in the upper part increased to two after cusp bifurcation ( $CP_1^U$ ).

#### 4. Discussion

In this study, we consider Stokes flow over Z-shaped cavity with moving upper lid. The matching biorthogonal eigenfunction expansions method which is used by (Trogon and Joseph 1982, Driesen et. al 1998) for rectangular slot, (Phillips 1989) for contraction geometry and (Deliceoğlu and Aydın 2014) for L-shaped cavity is applied here for the first time for the Z-shaped cavity. Then, flow structures occurring in the region by changing the height of the Z-shaped cavity are presented. The  $(h_1, h_2)$  control space

diagram was generated for  $-2.8 < h_1 < 0.1, 0 < h_2 < 2$ . The flow transformations in the cavity and the new vortex formation mechanism were examined by taking sections from different parts of the control space diagram. It is concluded that there is no new vortex in the upper part of the cavity unless the separation line exceeds the left corner point. It is surprising that after crossing the corner point of the separation line, the saddle-node bifurcation on the wall remains almost the same value  $h_2=1.62$ , regardless of  $h_1$ . This value is the same as that obtained for rectangular (Gürcan 2005) and L-shaped (Deliceoğlu and Aydın 2014) cavities with a single lid-driven by uniform motion. Thus, it was shown that this change in the shape of the flow field does not affect the formation of the vortex in the upper part of the cavity.

## 5. References

- An, B., Bergada, J.M., Mellibovsky, F. 2019.** The lid-driven right-angled isosceles triangular cavity flow. *J. Fluid Mech.*, 875(9), 476–519. <https://doi.org/10.1017/jfm.2019.512>
- Bakker, P.G. 1991.** Bifurcations in Flow Patterns. *In Kluwer*. <https://doi.org/10.1017/S0022112093211624>
- Botella, O., Peyret, R. 1998.** Benchmark Spectral Results on the Lid Driven Cavity Flow. *Comput. Fluids*, 27(4), 421–433. [https://doi.org/10.1016/S0045-7930\(98\)00002-4](https://doi.org/10.1016/S0045-7930(98)00002-4)
- Brøns, M., Hartnack, J. N. 1999.** Streamline topologies near simple degenerate critical points in two-dimensional flow away from boundaries. *Phys. Fluids*, 11(2), 314–324. <https://doi.org/10.1063/1.869881>
- Bruneau, C.H., Saad, M. 2006.** The 2D lid-driven cavity problem revisited. *Comput. Fluids*, 35(3), 326–348. <https://doi.org/10.1016/j.compfluid.2004.12.004>
- Deliceoğlu, A., Aydın, S.H. 2013.** Flow bifurcation and eddy genesis in an L-shaped cavity. *Comput. Fluids*, 73, 24–46. <https://doi.org/10.1016/j.compfluid.2012.12.008>
- Deliceoğlu, A., Aydın, S.H. 2014.** Topological flow structures in an L-shaped cavity with horizontal motion of the upper lid. *J. Comput. Appl. Math.*, 259(PART B), 937–943. <https://doi.org/10.1016/j.cam.2013.10.007>
- Deliceoğlu, A., Bozkurt, D., Çelik, E. 2019.** Flow topology in an L-shaped cavity with lids moving in the same directions. *Math. Methods Appl. Sci.*, 43(15), 8317–8326. <https://doi.org/10.1002/mma.5972>
- Deliceoğlu, A., Çelik, E. 2019.** A Mechanism of Eddy Generation in A Single Lid-Driven T-Shaped Cavity. *Cumhuriyet Science Journal*, 40(3), 583–594. <https://doi.org/10.17776/csj.569655>
- Driesen, C. H., Kuerten, J.G.M., Streng, M. 1998.** Low-Reynolds-number flow over partially covered cavities. *J. Eng. Math.*, 34(1–2), 3–21. [https://doi.org/10.1007/978-94-017-1564-5\\_1](https://doi.org/10.1007/978-94-017-1564-5_1)
- Erturk, E. 2018.** Benchmark solutions of driven polar cavity flow at high Reynolds numbers. *Int. J. Mech. Eng. Technol.*, 9(8), 776–786. Article ID: IJMET\_09\_08\_084
- Erturk, E., Corke, T.C., Gökçöl, C. 2005.** Numerical solutions of 2-D steady incompressible driven cavity flow at high Reynolds numbers. *Int. J. Numer. Methods Fluids*, 48(7), 747–774. <https://doi.org/10.1002/fld.953>
- Fadle, J. 1940.** Die Selbstspannungs-Eigenwertfunktionen der quadratischen Scheibe. *Ingenieur-Archiv*, 11(2), 125–149. <https://doi.org/10.1007/BF02084699>
- Gaskell, P.H., Savage, M.D., Summers, J.L., Thompson, H.M. 1995.** Modelling and analysis of meniscus roll coating. *J. Fluid Mech.*, 298(11), 113–137. <https://doi.org/10.1017/S0022112095003247>
- Gaskell, P.H., Savage, M.D., Wilson, M. 1997.** Stokes flow in a half-filled annulus between rotating coaxial cylinders. *J. Fluid Mech.*, 337(4), 263–282. <https://doi.org/10.1017/S0022112097005028>
- Gürçan, F. 2003.** Effect of the Reynolds number on streamline bifurcations in a double-lid-driven cavity with free surfaces. *Comput. Fluids*, 32(9), 1283–1298. [https://doi.org/10.1016/S0045-7930\(02\)00084-1](https://doi.org/10.1016/S0045-7930(02)00084-1)
- Gürçan, F., Bilgil, H., Şahin, A. 2016.** Bifurcations and eddy genesis of Stokes flow within a sectorial cavity PART II: Co-moving lids. *Eur. J. Mech. B. Fluids*, 56, 200–210. <https://doi.org/10.1016/j.euromechflu.2015.02.008>
- Gürçan, F., Gaskell, P.H., Savage, M.D., Wilson, M.C.T. 2003.** Eddy genesis and transformation of Stokes flow in a double-lid driven cavity. *Proc. Inst. Mech. Eng. C J. Mech. Eng. Sci.*, 217(3), 353–363. <https://doi.org/10.1243/095440603762870018>
- Gürçan, F., Wilson, M.C.T., Savage, M.D. 2006.** Eddy genesis and transformation of Stokes flow in a double-lid-driven cavity. Part 2: Deep cavities. *Proc. Inst. Mech. Eng. C J. Mech. Eng. Sci.*, 220(12), 1765–1773. <https://doi.org/10.1243/0954406JMES279>
- Gürçan, F. 2005.** Streamline topologies near a stationary wall of Stokes flow in a cavity. *Appl. Math. Comput.*, 165(2), 329–345. <https://doi.org/10.1016/j.amc.2004.06.017>
- Hartnack, J. N. 1999.** Streamline topologies near a fixed wall using normal forms. *Acta Mech.*, 136(1), 55–75. <https://doi.org/10.1007/BF01292298>
- Hellebrand, H. 2006.** Tape Casting. *Mater. Sci. Technol.* (eds R.W. Cahn, P. Haasen and E.J. Kramer) <https://doi.org/10.1002/9783527603978.mst0192>
- Hriberšek, M., Škerget, L. 2005.** Boundary domain integral method for high Reynolds viscous fluid flows in complex planar geometries. *Comput. Methods Appl. Mech. Eng.*, 194(39–41), 4196–4220. <https://doi.org/10.1016/j.cma.2004.11.002>
- Mahmoodi, M. 2011.** Numerical simulation of free convection of a nanofluid in L-shaped cavities. *Int. J. Therm. Sci.* <https://doi.org/10.1016/j.ijthermalsci.2011.04.009>
- Olsman, W.F.J., Colonius, T. 2011.** Numerical simulation of flow over an airfoil with a cavity. *AIAA Journal*, 49(1), 143–149. <https://doi.org/10.2514/1.J050542>
- Oztop, H.F., Dagtekin, I. 2004.** Mixed convection in two-sided lid-driven differentially heated square cavity. *Int. J. Heat Mass Transfer.*, 47(8–9), 1761–1769. <https://doi.org/10.1016/j.ijheatmasstransfer.2003.10.016>
- Papkovich, P.F. 1970.** Über eine Form der Lösung des byharmonischen Problems für das Rechteck. *Dokl. Acad. Sci. USSR.*, 27, 334–338.

- Phillips TN. 1989**, Singular Matched Eigenfunction Expansions for Stokes Flow around a Corner, *IMA J. Appl. Math.*, 42(1), 13–26. <https://doi.org/10.1093/imamat/42.1.13>
- Robbins, CI., Smith, RCT. (1948)**. CXIX. A table of roots of  $\sin Z = -Z$ . *The London, Edinburgh, and Dublin Philosophical Magazine and Journal of Science*, 39(299), 1004–1005. <https://doi.org/10.1080/14786444808521711>
- Shankar, PN. 1993**. The eddy structure in stokes flow in a cavity. *J. Fluid Mech.*, 250, 371–383. <https://doi.org/10.1017/S0022112093001491>
- Sheu, TWH., Chiang, CY. 2014**. Numerical investigation of chemotactic phenomenon in incompressible viscous fluid flow. *Comput. Fluids*, 103, 290–306. <https://doi.org/10.1016/j.compfluid.2014.07.023>
- Trogon, SA., Joseph, DD. 1982**. Matched eigenfunction expansions for slow flow over a slot, *J. Nonnewton Fluid Mech.*, 10(3–4), 185–213. [https://doi.org/10.1016/0377-0257\(82\)80001-3](https://doi.org/10.1016/0377-0257(82)80001-3)
- Yang, G., Sun, J., Liang, Y., Chen, Y. 2014**. Effect of Geometry Parameters on Low-speed Cavity Flow by Wind Tunnel Experiment. *AASRI Procedia*, 9, 44–50. <https://doi.org/10.1016/j.aasri.2014.09.009>